Available online at www.sciencedirect.com

SCIENCE DIRECT

Genomics 87 (2006) 84 – 92

GENOMICS

www.elsevier.com/locate/ygeno

A knock-in mouse model of congenital erythropoietic porphyria

C. Ged [a,*], M. Mendez [a,1], E. Robert [a], M. Lalanne [a], I. Lamrissi-Garcia [a], P. Costet [b], J.Y. Daniel [b,c], P. Dubus [d], F. Mazurier [a], F. Moreau-Gaudry [a], H. de Verneuil [a]

[a] *INSERM E217, Université Victor Segalen Bordeaux 2, 146 rue Léo Saignat, 33076 Bordeaux Cedex, France*

[b] *Animalerie Transgénique, Service Commun, Université Victor Segalen Bordeaux 2, 146 rue Léo Saignat, 33076 Bordeaux Cedex, France*

[c] *Laboratoire de Biologie du Développement et de la Différenciation, Université Victor Segalen Bordeaux 2, 146 rue Léo Saignat, 33076 Bordeaux Cedex, France*

[d] *EA 2406 Histologie et Pathologie Moléculaire, Université Victor Segalen Bordeaux 2, 146 rue Léo Saignat, 33076 Bordeaux Cedex, France*

Received 25 April 2005; accepted 27 August 2005
Available online 28 November 2005

Abstract

Congenital erythropoietic porphyria (CEP) is a recessive autosomal disorder characterized by a deficiency in uroporphyrinogen III synthase (UROS), the fourth enzyme of the heme biosynthetic pathway. The severity of the disease, the lack of specific treatment except for allogeneic bone marrow transplantation, and the knowledge of the molecular lesions are strong arguments for gene therapy. An animal model of CEP has been designed to evaluate the feasibility of retroviral gene transfer in hematopoietic stem cells. We have previously demonstrated that the knockout of the *Uros* gene is lethal in mice (*Uros*^{del} model). This work describes the achievement of a knock-in model, which reproduces a mutation of the *UROS* gene responsible for a severe UROS deficiency in humans (P248Q missense mutant). Homozygous mice display erythrodontia, moderate photosensitivity, hepatosplenomegaly, and hemolytic anemia. Uroporphyrin (99% type I isomer) accumulates in urine. Total porphyrins are increased in erythrocytes and feces, while Uros enzymatic activity is below 1% of the normal level in the different tissues analyzed. These pathological findings closely mimic the CEP disease in humans and demonstrate that the *Uros*^{mut248} mouse represents a suitable model of the human disease for pathophysiological, pharmaceutical, and therapeutic purposes.

Keywords: Animal model; Gene transfer; Günther's disease; Homologous recombination; Knock-in mice; Porphyria; Transgenic mice

Introduction

Congenital erythropoietic porphyria (CEP) is a rare disease that is inherited as an autosomal recessive trait and characterized biochemically by a massive porphyrinuria resulting from the accumulation in the bone marrow, peripheral blood, and other organs of large amounts of predominantly type I porphyrins. The diagnosis can be confirmed by the demonstration of a profound deficiency of uroporphyrinogen III synthase (UROS; EC 4.2.1.75) enzymatic activity in erythrocytes and other tissues [1,2]. The determination of the nucleotide sequence of the cDNA encoding UROS [3] has made possible the study of the molecular lesions responsible for the disease [2,4–14]. In most of the patients, the prognosis is poor and death occurs in early adult life. However, some variability exists in the expression of the disease, varying from extremely severe neonatal to mild late-onset forms [1,2,11,12].

Current available treatments are only symptomatic and unsatisfactory. Because the predominant site of metabolic expression of the disease is the erythropoietic system, bone marrow transplantation represents a curative treatment for patients with severe phenotypes, when a HLA-compatible donor is available [1,2,15]. The development of a mouse model of the disease will permit ex vivo gene therapy experiments on the entire animal.

The data shown in this report demonstrate that the *Uros*^{mut248} knock-in mouse represents a valuable model of the human UROS deficiency disease (CEP).

* Corresponding author. Fax: +33 5 56 98 33 48.
E-mail address: cecile.ged@u-bordeaux.fr (C. Ged).
[1] Present address: Centro de Investigacion, Hospital 12 de Octubre, Madrid, Spain.

0888-7543/$ - see front matter © 2005 Elsevier Inc. All rights reserved.
doi:10.1016/j.ygeno.2005.08.018

Results

Targeting of the Uros gene in ES cells and generation of transgenic mutant mice

The targeting construct represents 6.22 kb of mouse genomic DNA and contains the last two exons of the *Uros* gene (exons 9 and 10). Fig. 1 shows the targeting strategy: the homologous recombination between the targeted locus and the targeting construct leads to a modified gene that contains the positively selectable gene *neo*^{r}, which replaces a 0.9-kb piece of the 9th intron of the *Uros* gene. The P248Q missense mutation, encoded by a CCA → CAA change, is located in exon 10. The targeting construct contains a copy of the negatively selectable marker, herpes simplex thymidine kinase gene (*HS-TK*), which allows the use of a positive–negative selection of homologous recombinant ES clones. Two hundred five double-resistant ES clones were successfully amplified. The screening for the targeting event (Fig. 1) included PCR with different sets of primers along and outside the targeted locus, Southern blot, sequencing of exon 10, and Uros enzymatic assay. Five independent ES clones were characterized as homologous recombinants by PCR and Southern blot but only two contained the P248Q mutation and showed a 50% decrease in Uros enzymatic activity. After blastocyst reimplantations, 10 viable chimeras were obtained and 6 gave germ-line

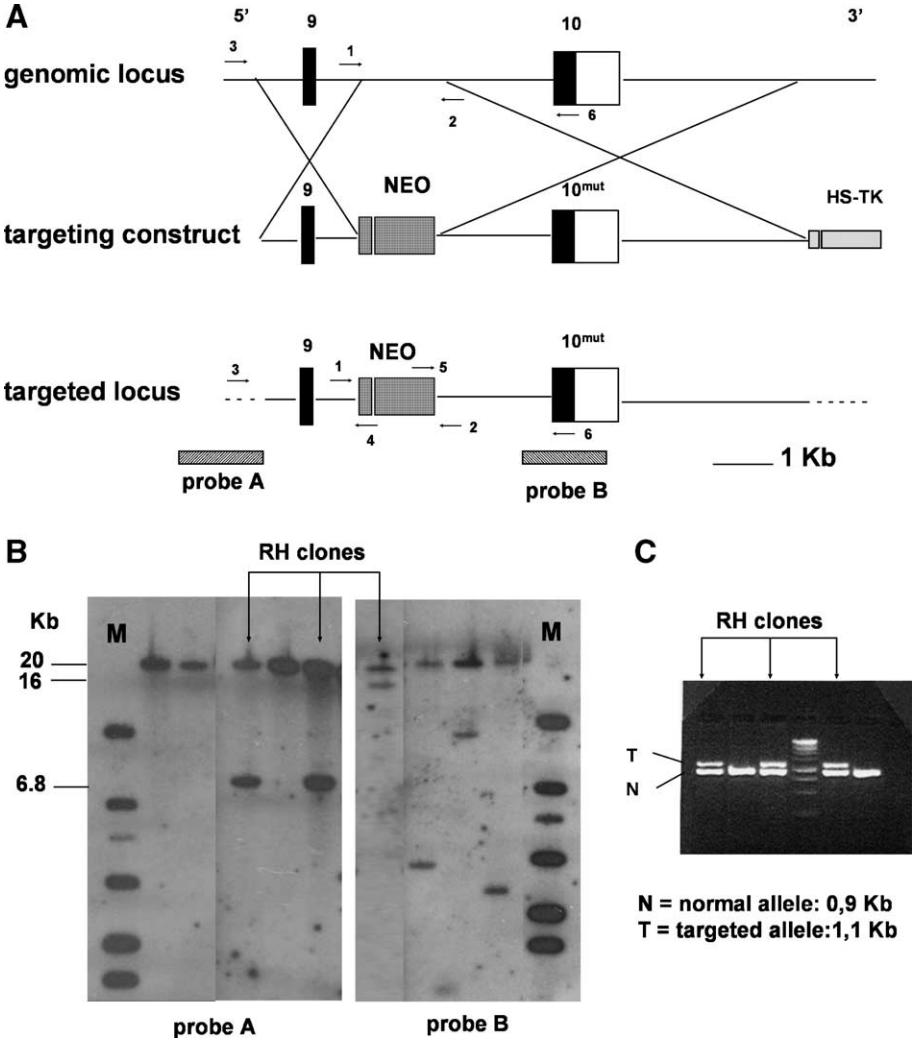

Fig. 1. (A) Targeting construct and (B, C) *Uros* gene analysis in ES cells. The targeting construct used to electroporate ES cells is shown in panel A. Top: Parental genomic locus containing the 9th and 10th exons of the mouse *Uros* gene. Middle: Targeting construct including the selective markers *neo*® and *TK* in the replacement vector. Bottom: Resulting targeted locus. The region of homology is shown by crossing lines on each side of the *neo* cassette. The positions of the probes used in Southern blot analyses are shown under the targeted construct. The primers used in PCR assays are shown by small arrows on the corresponding gene fragments. Homologous recombination was assessed by Southern blot analysis in ES cells, as shown in panel B. In *Eco*RI digests, probes A and B each recognized two bands in homologous recombinant ES cells, 6.8 and 20 kb (probe A) or 16 and 20 kb (probe B), corresponding to the targeted and normal allele, respectively. When random integration occurred, probe A gave a single band (20 kb), while probe B gave two bands, a common (20 kb) and a variable sized band, due to random integration (the *Eco*RI restriction site is located in the *neo* cassette and absent in the normal allele at the targeted locus). A typical profile of the PCR fragments generated with the (1, 2) primer set is shown in panel C. In heterozygous ES cells, two PCR products were obtained, 0.9 and 1.1 kb, corresponding to the normal and the *neo* allele, respectively. The same PCR was used for genotyping on mouse tail biopsies.

Table 1
Comparison of liver and spleen weight with reference to body weight (BW) in 6-month-old mice

Genotype	*n*	BW (g)	Liver (g)	Spleen (g)	Liver/BW (%)	Spleen/BW (%)
Mut/Mut	5	27.8 ± 5.1	2.01 ± 0.39	0.77 ± 0.18	7.26 ± 0.94	2.9 ± 1.08
p[a]		NS	<0.005	<0.005	<0.005	<0.005
Mut/N	6	29.2 ± 5.5	1.39 ± 0.39	0.12 ± 0.12	4.66 ± 0.86	0.43 ± 0.12
p[b]		NS	NS	NS	NS	NS
N/N	6	30.8 ± 4.5	1.34 ± 0.26	0.10 ± 0.16	4.40 ± 0.82	0.30 ± 0.11

[a] *Mut/Mut* vs *N/N*.
[b] *Mut/N* vs *N/N*.

transmission after breeding with wild-type mice. Finally, 17 heterozygous mice out of 63 births were characterized. The intercrosses between these heterozygous mice gave 59 births from 16 litters. The following frequencies were observed: 18.6% (11/59), 44.1% (26/59), and 37.3% (22/59) in the *Uros*$^{P248Q/P248Q}$ (*Mut/Mut*), *Uros*$^{P248Q/N}$ (*Mut/N*), and *Uros*$^{N/N}$ (*N/N*) genotypes, respectively.

Clinical features of the model

Heterozygous mice (*Mut/N*) appeared normal. Homozygous mice (*Mut/Mut*) were hypotrophic at birth and recognizable by producing red urine and showing erythrodontia in the first weeks of life. Later on, no difference in body weight was noted in homozygous mice compared to normal or heterozygous siblings (Table 1). Photosensitivity lesions of the ears and the back of the neck were observed in homozygous mice after several months of life. The examination after laparotomy showed enlarged liver and spleen and a brownish coloration of these organs, due to the accumulation of porphyrins. Bones were abnormally fragile and remained intensely colored after bone marrow aspiration (Fig. 2).

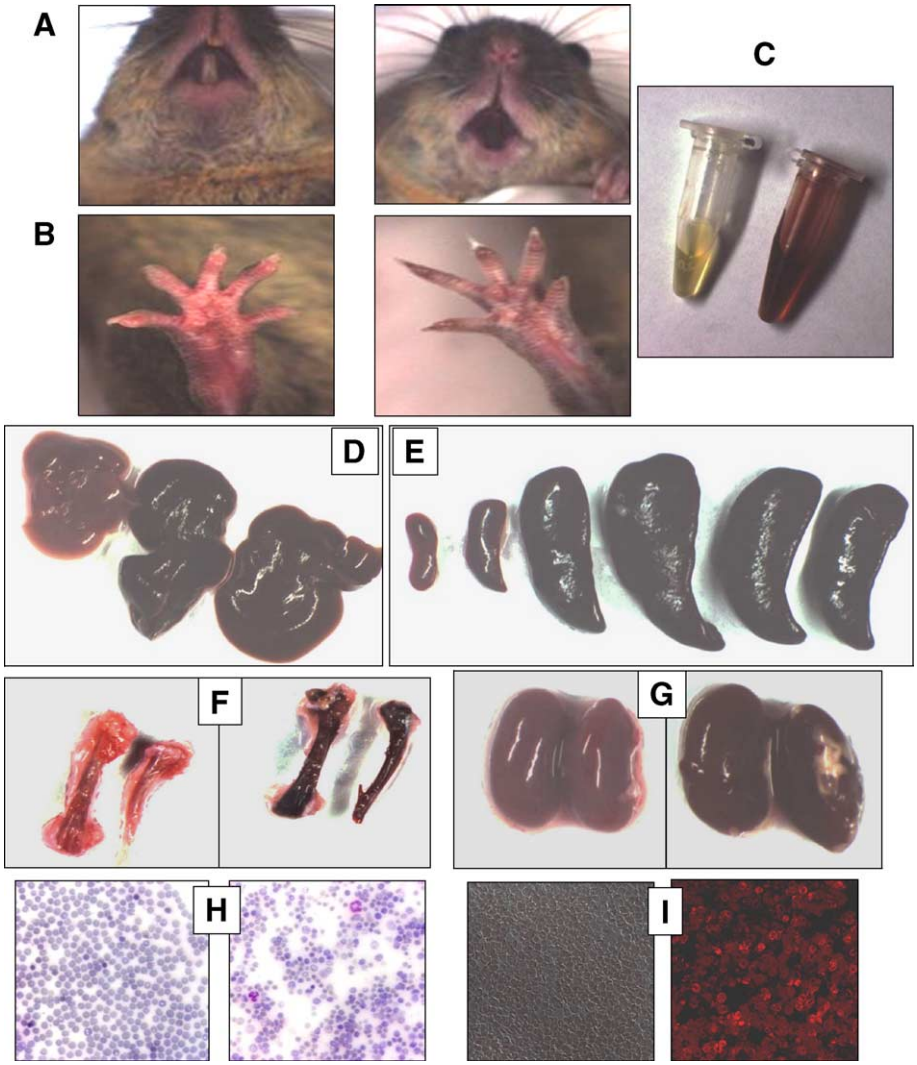

Fig. 2. Clinical features of the mouse model. Physical examination of homozygous mice (right side of each panel) compared to normal litters (left side) showed (A) erythrodontia, (B) discolored fingers due to anemia, (C) red-colored urine, and (D) liver and (E) spleen enlargement. Liver, spleen, (F) bones, and (G) kidneys had a reddish-brown color on daylight exposure. (H) Blood spread showed that red blood cells varied in size (anisocytosis) and pigment content (polychromasia) and were mainly discolored (hypochromia). (I) Microscopic examination under UV light evidenced numerous fluorocytes.

Biochemical and hematological studies

Porphyrin studies demonstrated a massive accumulation of total porphyrins in blood, urine, and feces (Table 2). In UROS deficiency, the majority of hydroxymethylbilane (linear tetrapyrrole) is converted into uroporphyrinogen I by a spontaneous cyclization (Fig. 3). In urine, the accumulation of uroporphyrin consisted in 99.5% of the type I isomer. Uroporphyrinogen I is partly converted into coproporphyrinogen I by the next enzyme of the heme pathway (uroporphyrinogen decarboxylase), and low amounts of intermediates harboring seven, six, or five carboxylic acid groups are found in the urine (Table 2). Hepatic (20.76 ± 5.66 nmol/g protein) and splenic (17.78 ± 11.86) porphyrin accumulation increased 15- and 50-fold, respectively, in homozygous animals compared to normal porphyrin levels (1.37 ± 1.1 and 0.36 ± 0.19). In heterozygous animals, porphyrin levels were similar to the normal levels in all tissues examined.

Uros enzymatic activity in erythrocytes was about 50% (8.19 ± 2.92 U/mg protein) and less than 1% (<0.1 U/mg) of the control level (12.51 ± 2.92 U/mg) in heterozygous and homozygous mice, respectively.

Hepatic parameters showed normal total bilirubin and alkaline phosphatase levels, and a slight increase in transaminase levels (two- to fourfold) in homozygous animals.

Hematological data are shown in Table 3. Homozygous mice had a severe microcytic and hypochromic anemia. The hemolytic process was evidenced by the high reticulocyte count and the presence of numerous erythroblasts with poikilocytosis and anisochromia, on microscopic examination. Flow-cytometric analysis of peripheral red blood cells showed that 10 to 30% of cells presented with abnormal porphyrin-mediated fluorescence (Fig. 4). Remarkably, the fluorocytes were mostly in the reticulocyte fraction, as characterized by orange thiazol dye.

Table 2
Porphyrin accumulation in red blood cells, urine, and feces

	Mut/Mut (n = 5)	*Mut/N* (n = 6)	*N/N* (n = 6)
Red blood cells (pmol/mg Hb)	72.06 ± 44.96	3.77 ± 0.47	3.95 ± 1.6
Urine			
Total porphyrins (μmol/L)	498 ± 328	<0.5	<0.5
Uroporphyrin (%)	88.6 ± 2.3	ND	ND
Heptacarboxylic porphyrin (%)	3.1 ± 1.0	ND	ND
Hexacarboxylic porphyrin (%)	1.0 ± 0.1	ND	ND
Pentacarboxylic porphyrin (%)	2.7 ± 0.3	ND	ND
Coproporphyrin (%)	4.7 ± 1.4	ND	ND
Uroporphyrin I (%)	≥99.5	ND	<20
Uroporphyrin III (%)	≤0.5	ND	>80
Fecal porphyrins (nmol/g)	185 ± 67	<10	<10

Histologic studies

Histological examination of bone marrow and spleen revealed an increase in erythroid precursor cells that paralleled the enlargement of the splenic red pulp. In the liver, several erythroid clusters were also noted and were associated with a mild centrilobular steatosis. Multifocal accumulation of a brown pigment was observed mainly in Kupffer cells and corresponded to iron deposits as attested by Perls staining.

In kidney, part of the glomeruli and tubules were filled by an eosinophilic material, which tended to enlarge the lumens. Again, a cortical brown pigmentation due to iron accumulation in the epithelial layer of the proximal convoluted tubules was evidenced by Perls staining (Fig. 5). Iron deposits in all these organs are probably linked to a sustained hemolytic process.

Discussion

In a previous work, we have demonstrated that homozygous $Uros^{del}$ embryos are nonviable from the earliest stage of development, i.e., blastocyst [16]. The finding that the disruption of the *Uros* gene is fully lethal is not surprising since the Uros enzyme contributes to the biosynthesis of heme, which is an essential compound in any mammalian cell.

Two mouse knockout models of porphyria have been previously described: acute intermittent porphyria (AIP) and familial porphyria cutanea tarda (f-PCT), due to porphobilinogen deaminase and uroporphyrinogen decarboxylase (UROD) deficiency, respectively [17,18]. In both models, the disruption of the gene was lethal in homozygous offspring. However, the genetic backgrounds are different; the corresponding human diseases are inherited in an autosomal dominant way and other genetic or environmental factors are necessary for the expression of the disease. In the mouse AIP model, neurological abnormalities were observed after phenobarbital administration in compound heterozygous animals. The animal model was designed mainly for a pathophysiological purpose [19]. In the mouse f-PCT model, $Urod^{+/-}$ mice did not accumulate hepatic porphyrins, while $Urod^{+/-}/Hfe^{-/-}$ mice developed a porphyric phenotype by 14 weeks of age, due to the addition of the $Hfe^{-/-}$ mutant modifier gene [18].

In CEP patients, the correlation between the phenotype and the genotype is well established [2]. The mutations responsible for the disease consist in nonsense and missense mutations, insertions, splicing defects, and base changes in the promoter of the *UROS* gene. No large deletion has been observed and a significant percentage of residual activity is always maintained.

In this work, the knock-in strategy was chosen to obtain a viable mutant phenotype in mice. The P248Q missense mutation has been shown to cause a severe phenotype in homozygous patients and a profound enzyme deficiency [2]. The structure of the *UROS* gene is very similar in human and mouse: the same exon–intron structure, the same size of coding sequences, and a single nucleotide change reproduced the mutation in the mouse sequence as well as in humans [20–23]. The expression of a P248Q mutant mouse Uros cDNA analyzed in a prokaryotic system (*Escherichia coli*) showed that the enzymatic activity of

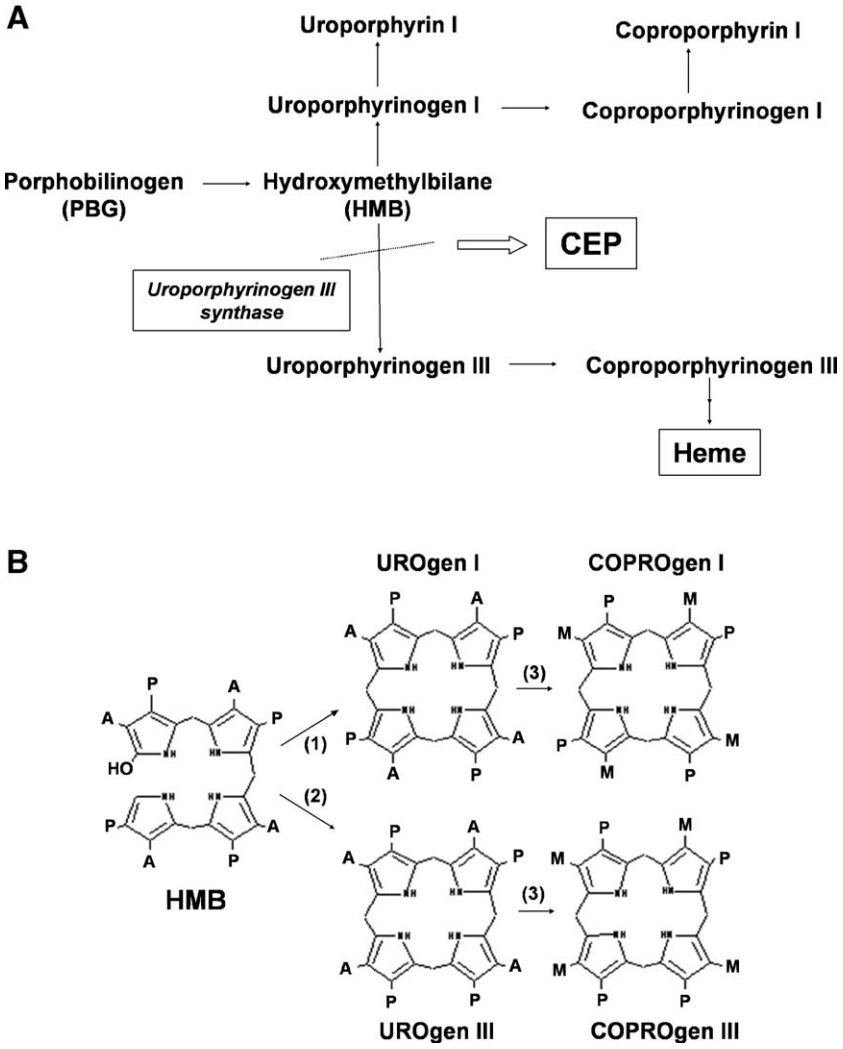

Fig. 3. Enzyme deficiency in CEP. (A) The enzyme deficiency present in CEP leads to the accumulation of uroporphyrin I and coproporphyrin I. Coproporphyrinogen I is not a substrate for the subsequent reactions of heme synthesis. Uro- and coproporphyrinogen I are oxidized into porphyrins I, accumulate in tissues, and are excreted in urine and feces. (B) In the presence of uroporphyrinogen III synthase (2), hydroxymethylbilane (HMB) is converted into uroporphyrinogen III (UROgen III). In the absence of the enzyme (1), HMB is converted into uroporphyrinogen I (UROgen I). Uroporphyrinogen decarboxylase (3) catalyzes the transformation of UROgen I and III into COPROgen I and III, respectively.

the resulting mutant Uros protein was 1% of the level of the corresponding normal Uros cDNA. This finding was in agreement with previous results in the same prokaryotic expression system using human UROS cDNA [11].

As expected, in the *Uros*^{mut248} knock-in model, heterozygous mice appeared normal, while homozygous mice had a typical porphyric phenotype as can be seen from the biochemical and hematological data. A dramatic increase in porphyrin level was found in red blood cells, urine, and feces, a typical feature of a severe CEP form in humans. Chronic anemia, due to excessive hemolysis, was detected on the first blood examination and had no influence on mouse development or behavior. The presence of numerous fluorocytes among the reticulocyte fraction of red blood cells was a typical hallmark of the disease and a convenient diagnosis test in this mouse model. The development of photosensitivity lesions was delayed and well tolerated without evident infected and scarring lesions.

Table 3
Hematological parameters in 6-month-old mice

	Mut/Mut (n = 5)	*Mut/N* (n = 6)	*N/N* (n = 6)
Hb (g/dl)	7.94 ± 0.46	13.24 ± 0.84	13.21 ± 1.17
RBC (10^{12}/L)	6.35 ± 0.95	8.5 ± 0.81	8.49 ± 0.73
MCV (fl)	39.52 ± 2.05	48.57 ± 3.42	48.13 ± 2.03
MCH (pg)	12.78 ± 1.74	15.63 ± 0.83	15.58 ± 0.70
MCHC (g/dl)	31.92 ± 3.25	32.22 ± 0.69	32.38 ± 0.73
Platelets (10^9/L)	524.98 ± 490.16	565.17 ± 275.13	535.67 ± 248.07
Reticulocytes (%)	29.72 ± 6.41	5	5
Fluorocytes (%)	20.90 ± 7.02	<0.5	<0.5

The availability of a mouse model of UROS deficiency represents a powerful tool for gene regulation studies, pathophysiological analyses, and therapeutic purposes [24].

The understanding of *UROS* gene regulation is partial. In mouse and human, tissue-specific expression is ensured by two distinct promoter regions: erythroid and housekeeping sequences have been described in erythroid and nonerythroid cells [22,23]. In the recent description of a large CEP family, different siblings had severe clinical manifestations, while one

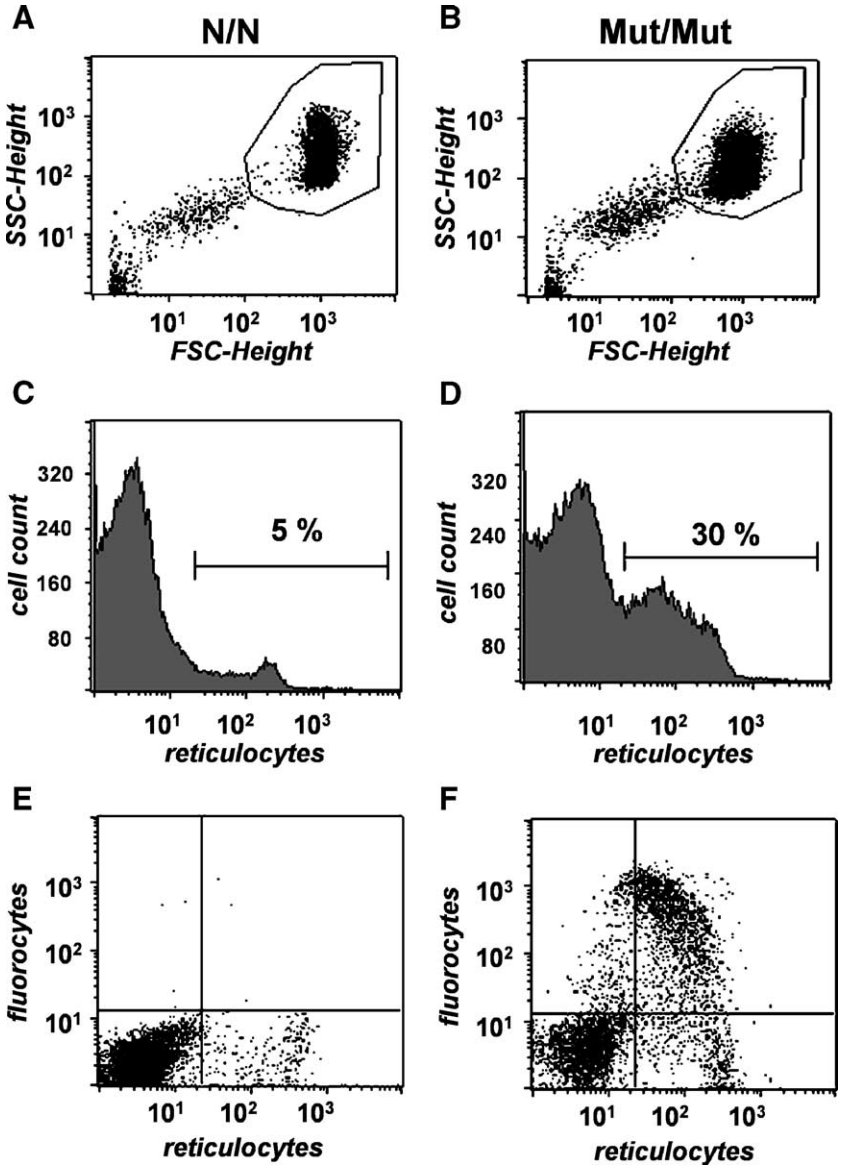

Fig. 4. Flow-cytometric analysis of fluorocytes and reticulocytes. (A and B) Selection of the red blood cell population by gating with side scatter (SSC-height) and forward scatter (FSC-height) in normal (A) and homozygous mice (B). (C and D) Histogram drawings of the reticulocyte population in normal (C) and homozygous mice (D). (E and F) Analysis of the reticulocyte fraction by orange thiazol labeling (x axis, FL-1 channel) and of the fluorocyte fraction by red fluorescence (y axis, FL-3 channel) in normal (E) and homozygous mice (F). Fluorocytes are mainly in the reticulocyte fraction.

homozygous mutant sibling was clinically healthy [14]. This observation led to the hypothesis of a putative modifier gene responsible for the phenotypic variability. The same hypothesis has recently been documented in a mouse model of erythropoietic protoporphyria, the *Fech*$^{m1Pas/m1Pas}$ mouse, obtained by chemical mutagenesis [25]. The study performed on three congenic strains provides strong evidence for an independent genetic control of bone marrow contribution to porphyrin overproduction [26]. Our mouse model of CEP is a valuable tool to investigate the phenotypic variability in UROS deficiency.

A second field of interest is the possibility of ex vivo and in vivo gene therapy experiments. We and others have documented a sufficient in vitro gene transfer rate and metabolic correction in different CEP deficient cells to indicate that the disease is a good candidate for treatment by gene therapy in hematopoietic stem cells [27–30]. Experimental gene therapy has proven successful in the *Fech*$^{m1Pas/m1Pas}$ mouse [31–33]. Our latest results demonstrated that correction and in vivo expansion of deficient hematopoietic stem/progenitor cells can be achieved by a dual gene therapy involving the therapeutic gene and the methylguanine-DNA-methyltransferase-mediated selection system [34]. The recently developed lentivectors will be tested for gene transfer experiments in our mouse model of CEP as a last step before a gene therapy proposal in humans.

Materials and methods

Construction of the targeting vector

The P248Q missense mutation was introduced by site-directed mutagenesis in a 1.7-kb *Bam*HI genomic fragment that contains exon 9. A single base change (C → A) was created by using the Gene Editor Site

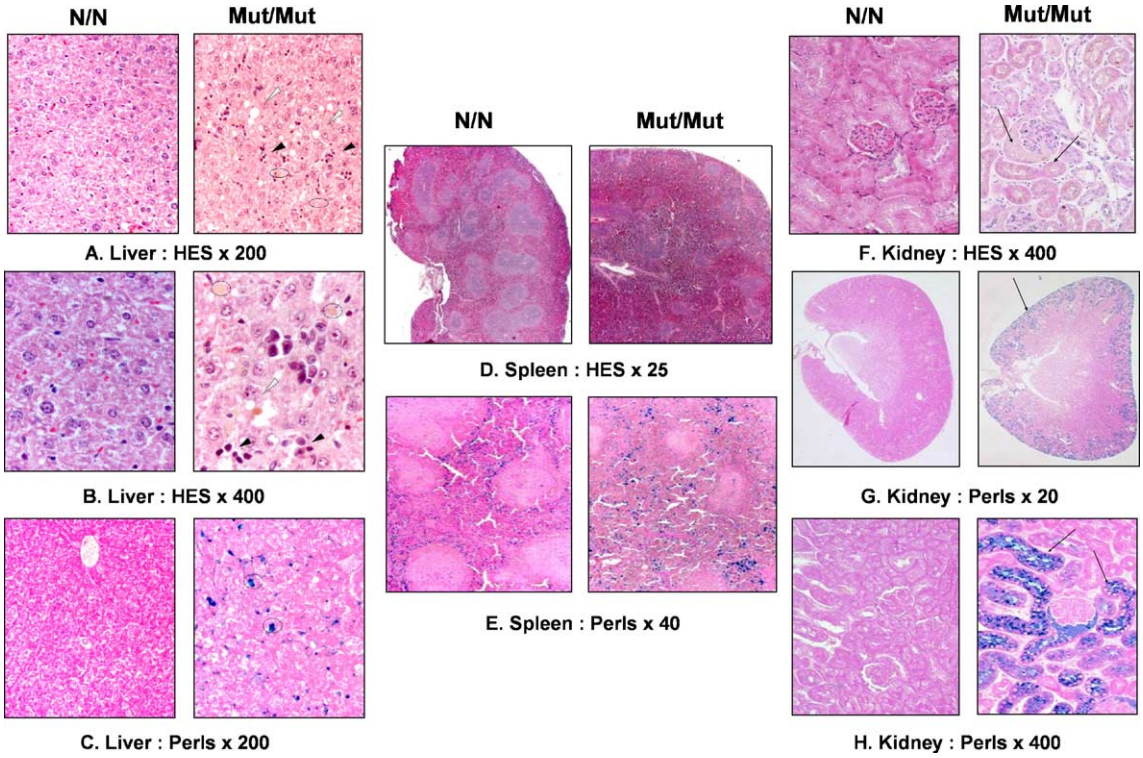

Fig. 5. Histologic analyses of liver, spleen, and kidneys. Normal liver, spleen, and kidneys are shown on the left of each slide. (A–C) Liver histology showed steatosis (gray arrowheads), clusters of erythroid cells in the sinusoids (black arrowheads), and pigment accumulation (dotted circles) due to iron deposits. (D) In spleen, the red pulp is enlarged and filled by erythroid precursor cells at a small magnifying scale; (E) iron deposits were intense in homozygous animals, seen by Perls staining. (F) Kidney analyses showed glomerular and tubular accumulation of a hyaline material (black arrows). (H, G) Perls staining identified iron deposits (black arrows) which predominate in the proximal convoluted tubules of the kidney's cortex.

Directed Mutagenesis kit (Promega, France) in the genomic fragment cloned into pBluescript plasmid (Clontech, France). The targeting construct prepared to obtain the *Uros*^{del} KO model [16] was modified as follows: the 1.7-kb mutant fragment was cloned at *Xho*I restriction sites after partial filling to obtain compatible ends with *Bam*HI in the KO construct; the new genomic fragment replaced the previously deleted one (the previous deletion removed the 3′ moiety of exon 9 and 0.8 kb of the adjacent intron). The targeting vector contained the *neo* expression cassette from pMC1Neo plasmid and the *HS-TK* cassette from pKSHT87S plasmid as previously described [16].

Targeted disruption of the Uros gene in ES cells

H_1ES cells were cultured on inactivated embryonic fibroblasts in DMEM supplemented with leukemia inhibitory factor by standard methods [35,36]. The construct was electroporated into *Uros*$^{N/N}$ cells to generate *Uros*$^{Mut/N}$ cell lines: 10 μg of the linearized targeting vector was electroporated into 10^7 H_1ES cells at room temperature using a Gene Pulser II system (Bio-Rad, France). The selection with G418 (150 μg/ml) and ganciclovir (2 μmol/L) was maintained for 10 days. Double-resistant colonies were picked, expanded, and analyzed for the presence of the recombination event by Southern blot, PCR, and sequencing of the mutant exon. Chromosomal distribution was checked by karyotypic analysis.

Generation of transgenic mice

Chimeric mice were generated by microinjection of homologous recombinant ES cells into 129/SV blastocysts, which were implanted into the uterine horn of pseudopregnant foster mothers. Chimeras were mated with C57BL/6 wild-type females to facilitate the analysis of the germ-line transmission from coat color. The offspring were analyzed for the presence of the mutant *Uros*^{P248Q} allele, and the first heterozygous animals were interbred to generate homozygous *Mut/Mut* mice. These animals had a mixed 129/SV–C57BL/6 genetic background. Animals were maintained on a 12-h light/dark cycle and had free access to food and water. All procedures involving animals were in accordance with the guidelines for humane care of laboratory animals.

Uros gene analysis in ES cells and tail biopsies

DNA was prepared from ES cells and tail biopsies by lysis followed by phenol–chloroform extraction. In Southern blot analyses, 10 μg of genomic DNA was digested with *Eco*RI enzyme, size-fractionated by electrophoresis, and successively hybridized with two ^{32}P-labeled probes: probe A is a 1.5-kb *Sac*I genomic fragment located on the 5′ side of the targeted locus in the 8th intron of the mouse *Uros* gene; probe B is a 1.3-kb *Hin*dIII genomic fragment containing the 10th exon of the mouse *Uros* gene (Fig. 1).

Three primer sets (1/2, 3/4, 5/6) were used for PCR analyses as shown by the arrows in Fig. 1. Primers 1 and 2 are located on each side of the *neo* cassette. The size of the amplified fragment differs in the normal and the mutant allele, 0.9 and 1.1 kb, respectively. Primer sequences are (1) 5′-CTTATGCTAGTCT-GGTTGTG-3′ and (2) 5′-GCTCAGGTCAGAAGTCACTC-3′. Amplification with primers 3 and 4 demonstrates the targeting event: the 1.6-kb fragment observed is specific for the targeted locus. Primer sequences are (3) 5′-GGTTCTGTCATTTCCAGCCA-3′ and (4) 5′-AGGCTTTTTGCTTCC-TCTTG-3′. Primers 5 and 6 are located at the 3′ end of the *neo* cassette and the 3′ end of the 10th exon of the mouse *Uros* gene, respectively. The corresponding 0.9-kb fragment, observed in the mutant allele, was sequenced to check for the presence of the P248Q mutation. Primer sequences are (5) 5′-CCTGACGAGTTCTTCTGAGG-3′ and (6) 5′-TCAGCAACAGTGGTTT-GGCT-3′.

The hot-start Gold *Taq* polymerase (Perkin–Elmer, France) was used for PCR analyses. PCR products were purified on Qiaquick columns (Qiagen, France) before direct sequencing using the BigDye Terminator Cycle Sequencing kit on the ABI377 automated sequencer (Applied Biosystems, France).

Biochemical and hematological measurements

Blood was collected by puncture of the orbital sinus. The usual biochemical parameters, total bilirubin, transaminases, and alkaline phosphatases, were measured using a CX7 (Beckman Coulter France SA, Villepinte, France). Hematological parameters were measured in a Coulter counter (Beckman Coulter). Porphyrin levels in blood and organs were determined spectrofluorimetrically using a Hitachi F-4500 fluorescence spectrophotometer (Braun Sciencetec, France) [37]. Urinary and fecal porphyrin concentrations were analyzed by spectrophotometry after solvent extraction. The separation and the quantification of the different porphyrins and the uroporphyrin isomers was done by reversed-phase HPLC [38]. Uroporphyrinogen III synthase activity was determined by an enzyme-coupled assay as described previously [28]. One unit was defined as the amount of enzyme that formed 1 nmol of uroporphyrinogen III per hour at 37°C.

Flow-cytometric analysis

Analyses of porphyrin-accumulating cells in peripheral blood and bone marrow were performed with a FACS Calibur (BD Biosciences, Le Pont de Claix, France). Porphyrin fluorescence was detected in the FL-3 channel. Reticulocytes were labeled with orange thiazol and counted in the FL-1 channel.

Histology

Liver, spleen, and kidneys were examined after formaldehyde fixation, paraffin embedding, and different stainings: hematein–eosine–safran, Perls, and Schiff periodic acid. Blood and bone marrow cell spreads were analyzed by microscopic fluorescence and direct microscopy after May–Grundwald–Giemsa staining.

Statistical analyses

Student's paired t tests were used for comparison between heterozygous, homozygous, and control mice.

Acknowledgments

We are indebted to M. Lemeur, A. Dierich, and P. Chambon (Institut de Génétique et de Biologie Moléculaire et Cellulaire, CNRS/INSERM/ULP, Collège de France, Parc d'Innovation, BP 163, 67404 Illkirch Cedex, France) for their collaboration in obtaining the transgenic mice. We thank M.T. Sanchez for secretarial assistance.

This work was supported by the Conseil Régional d'Aquitaine and Association Française contre les Myopathies.

References

[1] K.E. Anderson, S. Sassa, D.F. Bishop, R.J. Desnick, Disorders of heme biosynthesis: X-linked sideroblastic anemia and porphyries, in: C.R. Scriver, A.L. Beaudet, E. Valle, W.S. Sly (Eds.), The Metabolic and Molecular Bases of Inherited Disease, McGraw–Hill, New York, 2001, pp. 2961–3062.

[2] H. de Verneuil, C. Ged, F. Moreau-Gaudry, Congenital erythropoietic porphyria, in: K.M. Kadish, K.M. Smith, R. Guilard (Eds.), The Porphyrin Handbook, vol. 14, Academic Press, New York, 2003, pp. 43–63.

[3] S.F. Tsai, D.F. Bishop, R.J. Desnick, Human uroporphyrinogen III synthase: molecular cloning nucleotide sequence, and expression of a full-length cDNA, Proc. Natl. Acad. Sci. USA 85 (1988) 7049–7053.

[4] J.C. Deybach, H. de Verneuil, S. Boulechfar, B. Grandchamp, Y. Nordmann, Point mutations in the uroporphyrinogen III synthase gene in congenital erythropoietic porphyria, Blood 75 (1990) 1763–1765.

[5] S. Boulechfar, V. Da Silva, J.C. Deybach, Y. Nordmann, B. Grandchamp, H. de Verneuil, Heterogeneity of the mutations in the uroporphyrinogen III synthase gene in congenital erythropoietic porphyria, Hum. Genet. 88 (1992) 320–324.

[6] C.A. Warner, H.W. Yoo, A.G. Roberts, R.J. Desnick, Congenital erythropoietic porphyria: identification and expression of exonic mutations in the uroporphyrinogen III synthase gene, J. Clin. Invest. 89 (1992) 693–700.

[7] M. Bensidhoum, C. Ged, I. Hombrados, F. Moreau-Gaudry, R.S. Hift, P. Meissner, E.D. Sturrock, H. de Verneuil, Identification of two new mutations in congenital erythropoietic porphyria, Eur. J. Hum. Genet. 3 (1995) 102–107.

[8] W. Xu, C.A. Warner, R.J. Desnick, Congenital erythropoietic porphyria: identification and expression of 10 mutations in the uroporphyrinogen III synthase gene, J. Clin. Invest. 95 (1995) 905–912.

[9] W. Xu, K.H. Astrin, R.J. Desnick, Molecular basis of congenital erythropoietic porphyria: mutations in the human uroporphyrinogen III synthase gene, Hum. Mutat. 7 (1996) 187–192.

[10] K. Tanigawa, et al., A novel point mutation in congenital erythropoietic porphyria in two members of a Japanese family, Hum. Genet. 97 (1996) 557–560.

[11] A. Fontanellas, M. Bensidhoum, R. Enriquez de Salamanca, H. de Verneuil, C. Ged, A systematic analysis of the mutations of the uroporphyrinogen III synthase gene in congenital erythropoietic porphyria, Eur. J. Hum. Genet. 4 (1996) 274–282.

[12] L. Verstraeten, et al., Biochemical diagnosis of a fatal case of Günther's disease in a newborn with hydrops foetalis, Eur. J. Clin. Chem. Clin. Biochem. 31 (1993) 121–128.

[13] N. Takamura, et al., Novel point mutation in the uroporphyrinogen III synthase gene causes congenital erythropoietic porphyria of a Japanese family, Am. J. Med. Genet. 70 (1997) 299–302.

[14] C. Ged, et al., Congenital erythropoietic porphyria: report of a novel mutation with absence of clinical manifestations in a homozygous mutant sibling, J. Invest. Dermatol. 123 (2004) 589–591.

[15] S. Dupuis-Girod, et al., Successful match-unrelated donor bone marrow transplantation for congenital erythropoietic porphyria, J. Pediatr. 164 (2005) 104–107.

[16] M. Bensidhoum, et al., The disruption of mouse uroporphyrinogen III synthase (uros) gene is fully lethal, Transgenics 2 (1998) 275–280.

[17] R. Lindberg, et al., Porphobilinogen deaminase deficiency in mice causes a neuropathy resembling that of human hepatic porphyria, Nat. Genet. 12 (1996) 195–199.

[18] J.D. Phillips, et al., A mouse model of porphyria cutanea tarda, Proc. Natl. Acad. Sci. USA 98 (2001) 259–264.

[19] M.R. Franklin, J.D. Phillips, J.P. Kushner, Uroporphyria in the uroporphyrinogen decarboxylase-deficient mouse: interplay with siderosis and polychlorinated biphenyl exposure, Hepatology 36 (2002) 805–811.

[20] M. Bensidhoum, C. Ged, C. Poirier, J.L. Guénet, H. de Verneuil, The cDNA sequence of mouse uroporphyrinogen III synthase and assignment to mouse chromosome 7, Mamm. Genome 5 (1994) 728–730.

[21] W. Xu, C.A. Kozak, R.J. Desnick, Uroporphyrinogen-III synthase: molecular cloning, nucleotide sequence, expression of a mouse full-length cDNA, and its localization on mouse chromosome 7, Genomics 26 (1995) 556–562.

[22] G.I. Aizencang, et al., Uroporphyrinogen III synthase: an alternative promoter controls erythroid-specific expression in the murine gene, J. Biol. Chem. 275 (2000) 2295–2304.

[23] G.I. Aizencang, C. Solis, D.F. Bishop, C. Warner, R.J. Desnick, Human uroporphyrinogen-III synthase: genomic organization, alternative promoters, and erythroid-specific expression, Genomics 70 (2000) 223–231.

[24] A. Wynshaw-Boris, Model mice and human disease, Nat. Genet. 13 (1996) 259–260.

[25] S. Tutois, et al., Erythropoietic protoporphyria in the house mouse, J. Clin. Invest. 88 (1991) 1730–1736.
[26] M. Abitbol et al., A mouse model provides evidence that genetic background modulates anemia and liver injury in erythropoietic protoporphyria, Am. J. Physiol. 288 (2005) 1208–1246.
[27] F. Moreau-Gaudry, et al., Correction of the enzyme defect in cultured congenital erythropoietic porphyria disease cells by retroviral mediated gene transfer, Hum. Gene Ther. 6 (1995) 13–20.
[28] F. Moreau-Gaudry, F. Mazurier, M. Bensidhoum, C. Ged, H. de Verneuil, Metabolic correction of congenital erythropoietic porphyria by retroviral-mediated gene transfer into lymphoblastoid cell lines, Blood 85 (1995) 1449–1453.
[29] F. Moreau-Gaudry, et al., Correction of bone marrow cells in congenital erythropoietic porphyria by retroviral gene transfer, Hematol. Cell Ther. 38 (1996) 217–220.
[30] R. Kauppinen, et al., Congenital erythropoietic porphyria: prolonged high-level expression and correction of the heme biosynthetic defect by retroviral-mediated gene transfer into porphyric and erythroid cells, Mol. Genet. Metab. 65 (1998) 10–17.
[31] R. Pawliuk, et al., Long-term cure of the photosensitivity of murine erythropoietic protoporphyria by preselective gene therapy, Nat. Med. 7 (1999) 768–773.
[32] A. Fontanellas, et al., Successful therapeutic effect in a mouse model of erythropoietic protoporphyria by partial genetic correction and fluorescence-based selection of hematopoietic cells, Gene Ther. 8 (2001) 618–626.
[33] E. Richard, et al., Gene therapy of a mouse model of protoporphyria with a self-inactivating erythroid-specific lentiviral vector without preselection, Mol. Ther. 4 (2001) 331–338.
[34] E. Richard, et al., Hematopoietic stem cell gene therapy of murine protoporphyria by methylguanine-DNA-methyltransferase-mediated in vivo drug selection, Gene Ther. 11 (2004) 1638–1647.
[35] E.J. Robertson, Teratomas and Embryonic Stem Cells: A Practical Approach, IRL Press, Oxford, 1987.
[36] T. Lufkin, A. Dierich, M. LeMeur, M. Mark, P. Chambon, Disruption of the Hox1-6 homeobox gene results in defects in a region corresponding to its rostral domain of expression, Cell 66 (1991) 1105–1119.
[37] B. Grandchamp, et al., Studies of porphyrin synthesis in fibroblasts of patients with congenital erythropoietic porphyria and one patient with homozygous coproporphyria, Biochem. Biophys. Acta 629 (1980) 577–586.
[38] C.K. Lim, T.J. Peters, Urine and fecal porphyrin profiles by reversed–phase high performance liquid chromatography in the porphyries, Clin. Chim. Acta 139 (1984) 55–63.